Directional sideward emission from luminescent plasmonic nanostructures

Dick K. G. de Boer,[1,*] Marc A. Verschuuren,[1] Ke Guo,[2] A. Femius Koenderink,[2] Jaime Gómez Rivas,[3] and Said Rahimzadeh-Kalaleh Rodriguez[2,4]

[1]*Philips Research, High Tech Campus 4, 5656 AE Eindhoven, The Netherlands*
[2]*Center for Nanophotonics, FOM Institute AMOLF, 1098 XG Amsterdam, The Netherlands*
[3]*Dutch Institute for Fundamental Energy Research DIFFER, P.O. Box 6336, 5600 HH Eindhoven, The Netherlands*
[4]*Present address: Laboratoire de Photonique et de Nanostructures, LPN/CNRS, Route de Nozay, 91460 Marcoussis, France*
[*]*dick.de.boer@philips.com*

Abstract: Periodic arrays of metallic nanoparticles can be used to enhance the emission of light in certain directions. We fabricated hexagonal arrays of aluminium nanoparticles combined with thin layers of luminescent material and optimized period (275 nm) and thickness (1500 nm) to obtain sideward directional emission into glass for a wavelength band around 620 nm. The key physics is that the luminescent layer acts as a waveguide, from which light is emitted at preferential angles using diffractive effects. This phenomenon has applications in the field of solid-state lighting, where there is a desire for small, bright and directional sources.

OCIS codes: (160.2540) Fluorescent and luminescent materials; (250.5403) Plasmonics.

References and links

1. S. Roelandt, Y. Meuret, D. K. G. de Boer, D. Bruls, P. Van De Voorde, and H. Thienpont, "In- and outcoupling of light from a luminescent rod using a compound parabolic concentrator (CPC)," Opt. Eng. **54**(5), 055101 (2015).
2. A. G. Curto, G. Volpe, T. H. Taminiau, M. P. Kreuzer, R. Quidant, and N. F. van Hulst, "Unidirectional emission of a quantum dot coupled to a nanoantenna," Science **329**(5994), 930–933 (2010).
3. G. M. Akselrod, C. Argyropoulos, T. B. Hoang, C. Ciracì, C. Fang, J. Huang, D. R. Smith, and M. H. Mikkelsen, "Probing the mechanisms of large Purcell enhancement in plasmonic nanoantennas," Nat. Photonics **8**(11), 835–840 (2014).
4. H. Aouani, O. Mahboub, E. Devaux, H. Rigneault, T. W. Ebbesen, and J. Wenger, "Plasmonic antennas for directional sorting of fluorescence emission," Nano Lett. **11**(6), 2400–2406 (2011).
5. L. Langguth, D. Punj, J. Wenger, and A. F. Koenderink, "Plasmonic band structure controls single-molecule fluorescence," ACS Nano **7**(10), 8840–8848 (2013).
6. G. Lozano, D. J. Louwers, S. R. K. Rodriguez, S. Murai, O. T. A. Jansen, M. A. Verschuuren, and J. Gómez Rivas, "Plasmonics for solid-state lighting: enhanced excitation and directional emission of highly efficient light sources," Light Sci. Appl. **2**(5), e66 (2013).
7. S. R. K. Rodriguez, G. Lozano, M. A. Verschuuren, R. Gomes, K. Lambert, B. De Geyter, A. Hassinen, D. Van Thourhout, Z. Hens, and J. Gómez Rivas, "Quantum rod emission coupled to plasmonic lattice resonances: A collective directional source of polarized light," Appl. Phys. Lett. **100**(11), 111103 (2012).
8. G. Vecchi, V. Giannini, and J. Gómez Rivas, "Shaping the fluorescent emission by lattice resonances in plasmonic crystals of nanoantennas," Phys. Rev. Lett. **102**(14), 146807 (2009).
9. P. Törmä and W. L. Barnes, "Strong coupling between surface plasmon polaritons and emitters: a review," Rep. Prog. Phys. **78**(1), 013901 (2015).
10. S. R. K. Rodriguez, Y. T. Chen, T. P. Steinbusch, M. A. Verschuuren, A. F. Koenderink, and J. Gómez Rivas, "From weak to strong coupling of localized surface plasmons to guided modes in a luminescent slab," Phys. Rev. B **90**(23), 235406 (2014).
11. S. R. K. Rodriguez, A. Abass, B. Maes, O. T. A. Janssen, G. Vecchi, and J. Gómez Rivas, "Coupling bright and dark plasmonic lattice resonances," Phys. Rev. X **1**(2), 021019 (2011).
12. G. Lozano, G. Grzela, M. A. Verschuuren, M. Ramezani, and J. G. Rivas, "Tailor-made directional emission in nanoimprinted plasmonic-based light-emitting devices," Nanoscale **6**(15), 9223–9229 (2014).
13. M. Lunz, D. de Boer, G. Lozano, S. R. K. Rodriguez, J. Gomez Rivas, and M. A. Verschuuren, "Plasmonic LED device," Proc. SPIE **9127**, 91270N (2014).
14. J. Bures, *Guided Optics* (Wiley-VCH, Weinheim, 2009).
15. I. Sersic, C. Tuambilangana, and A. F. Koenderink, "Fourier microscopy of single plasmonic scatterers," New J. Phys. **13**(8), 083019 (2011).

#251615 Received 9 Oct 2015; revised 22 Dec 2015; accepted 26 Dec 2015; published 7 Jan 2016

16. J. Gómez Rivas, G. Vecchi, and V. Giannini, "Surface plasmon polariton-mediated enhancement of the emission of dye molecules on metallic gratings," New J. Phys. **10**(10), 105007 (2008).
17. COMSOL, www.comsol.com
18. A. Goetzberger and W. Greubel, "Solar energy conversion with fluorescent collectors," Appl. Phys. (Berl.) **14**(2), 123–139 (1977).
19. M. G. Debije and P. P. C. Verbunt, "Thirty years of luminescent solar concentrator research: solar energy for the built environment," Adv. Energy Mater. **2**(1), 12–35 (2012).
20. D. K. G. de Boer, D. J. Broer, M. G. Debije, W. Keur, A. Meijerink, C. R. Ronda, and P. P. C. Verbunt, "Progress in phosphors and filters for luminescent solar concentrators," Opt. Express **20**(10), A395–A405 (2012).
21. N. C. Giebink, G. P. Wiederrecht, and M. R. Wasielewski, "Resonance-shifting to circumvent reabsorption loss in luminescent solar concentrators," Nat. Photonics **5**(11), 694–701 (2011).

1. Introduction

Solid-state light sources are fast becoming prominent sources of artificial light. Most applications nowadays rely on the use of blue LEDs combined with suitable luminophores (e.g. phosphors) to make light of the desired color or white light with desired color quality. However, the angular distribution of the emitted light is in general omnidirectional (e.g. Lambertian) and not optimal for many applications. Often a directional source is desired, or rather a small source with a low étendue (i.e., source surface area times solid angle of emission divergence). For a spot light, for instance, a forward directed emission would be preferred. For other applications, sideward emission is preferable that enables injection of light in a light guide (cf. Fig. 1). If the light guide is surrounded by many of such sources, the light emitted by all sources adds up in a low étendue. This light will stay in the light guide until it is extracted. One application of such a light guide is a high-brightness source, where the light is collected from one narrow face of the light guide [1]. Another application is a light tile, where the light is extracted by outcoupling features on the large surface opposite to that containing the emissive structures.

Nanostructures can influence the emission pattern of a luminescent material. In particular, structures supporting localized surface plasmon resonances like single metal nanoparticles [2], more complicated nanoparticle structures [3], nanoapertures in metal films [4,5], and diffractive structures [6,7] have proven efficient at redirecting luminescence from single luminophores. In the case of isolated metal nanoparticles, the plasmon resonances provide high local fields close to the particles. These local resonances can be coupled to extended modes by structuring the surface of a substrate with a periodic array of such particles, a so-called plasmonic array. These extended modes can be diffracted waves propagating along the surface, the so-called Rayleigh anomalies, or waveguide modes in case there is a thin waveguiding layer on top of the substrate [8,9]. If the thin layer contains luminophores, the emission characteristics will depend on the details of the structure and can be tailored by designing it adequately. One important parameter in this design is the thickness of the layer, which will influence the confinement of waveguide modes. This confinement affects the strength with which the surface plasmon resonances couple to the more delocalized waveguide modes [10] and hence the intensity of emission. The shape and dimensions of the metallic particles can influence the emission characteristics to some extent [11], whereas the directions of emission are mainly determined by the array period and symmetry. In this respect, a hexagonal structure is more favorable than a square structure in case one desires a highly symmetric emission pattern [12]. These effects can be used for shaping the directionality of the emitted light at particular wavelength ranges, e.g. in the above-mentioned applications of solid-state light sources, consisting of an LED (or laser) combined with a luminescent layer [6,13].

In this paper, we demonstrate a method for making a small directional sideward emitting light source that enables incoupling of light in a light guide (thickness of the order of 1 mm). This is sketched in Fig. 1 (where extraction of light, which may occur at the bottom surface or at the edge, is not considered). We first discuss which kind of structure can be used for obtaining sideward emission that enables injection of light in a light guide (Section 2.1). Next, we show experiments with a Fourier microscope on luminescent layers combined with

#251615 Received 9 Oct 2015; revised 22 Dec 2015; accepted 26 Dec 2015; published 7 Jan 2016

hexagonal arrays of various pitches (Section 2.2). In Section 3, the thickness of the luminescent layer is optimized using electromagnetic simulations and the simulated results for the optimal thickness are compared with experiment. Section 4 gives conclusions.

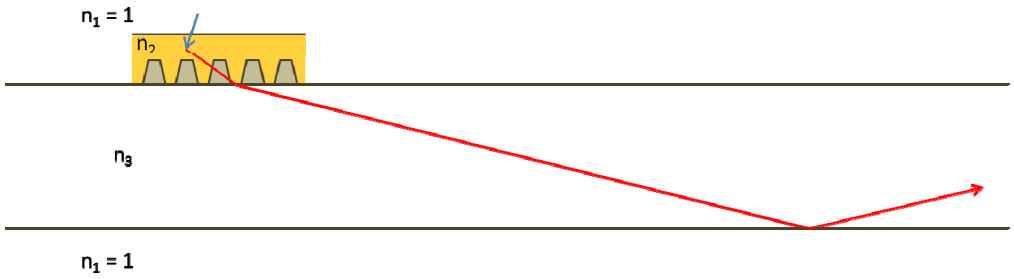

Fig. 1. Schematics of plasmonic phosphor-converted LED injecting light in a light guide (thickness approx. 1 mm) with index n_3. The LED light is converted in the phosphor layer with index n_2 which acts as a waveguide (thickness approx. 1 μm) and the plasmonic array makes that the converted light is emitted preferentially in directions that are in total internal reflection in the light guide with index n_3.

2. Period optimization

2.1 Theoretical considerations

In this Section, we assess the design of a structure with the desired directionality. First, we consider the preferred emission directions for luminophores adjacent to a hexagonal lattice. In Fig. 2(a), the dispersion diagram of the lattice, i.e., energy (along the vertical axis) vs the two components (k_x, k_y) of parallel wave vector, is shown in a repeated Brillouin-zone representation. The cones represent Rayleigh anomalies or waveguide modes, in zeroth (orange) and first order (grey). As mentioned before, a Rayleigh anomaly is a diffracted wave associated with diffraction into the sub- or superstrate, parallel to the surface of the grating surface. Both a Rayleigh anomaly and a waveguide mode result in a high electric field close to the grating.

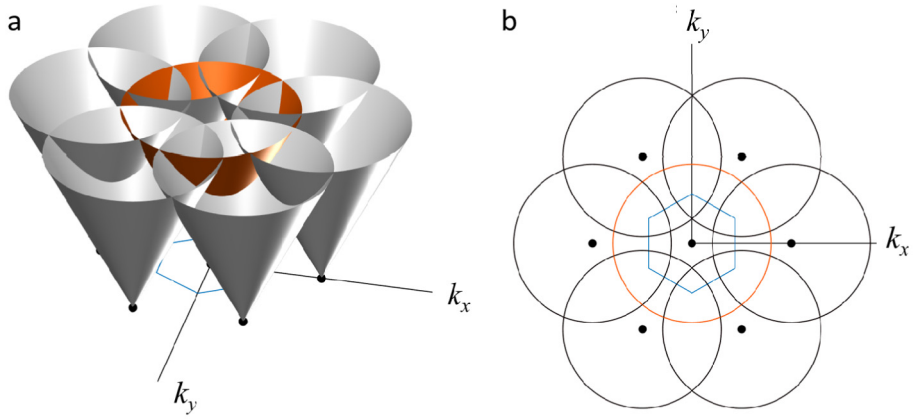

Fig. 2. (a) Diagram of energy vs two-dimensional parallel wave vector, showing resonances in reciprocal space for a waveguide coupled to a hexagonal lattice. (b) Horizontal cross section of Fig. 2(a) at energy corresponding to emission wavelength λ.

Figure 2(b) represents a horizontal cross section of Fig. 2(a) at certain energy, where the resonances show up as circles centered at the reciprocal lattice points. If this energy is the emission energy hc/λ of interest (where λ is the wavelength of emitted light), the radius of the

#251615 Received 9 Oct 2015; revised 22 Dec 2015; accepted 26 Dec 2015; published 7 Jan 2016

circles equals $n_{eff}\ 2\pi/\lambda$ (where n_{eff} is the index of the material supporting the Rayleigh anomaly or the effective waveguide mode index; see below).

The emission angle can be influenced by choosing a suitable period of the lattice, which is equivalent to tuning the diffraction condition. This corresponds to changing the size of the Brillouin zone (blue hexagon in Fig. 2). In Fig. 2(b), the circles correspond to directions in which the emission intensity is high.

Actually, Fig. 2 is simplified since it only shows one kind of resonance. In reality, Rayleigh anomalies can be supported by both the luminescent layer with index n_2 and the material with index n_3 (see Fig. 1). Moreover, several waveguide modes are supported by the luminescent layer, having effective indices in between n_2 and n_3. Figure 3 shows a cross section of Fig. 2 along k_x showing the dispersion of the modes in detail, with the waveguide modes (thin lines) in between the Rayleigh anomalies (dotted lines). The calculations [14] were done for numerical values corresponding to the experimental case described below. In Fig. 3, the horizontal red line represents the emission energy of interest, corresponding to the horizontal cross section shown in Fig. 2(b).

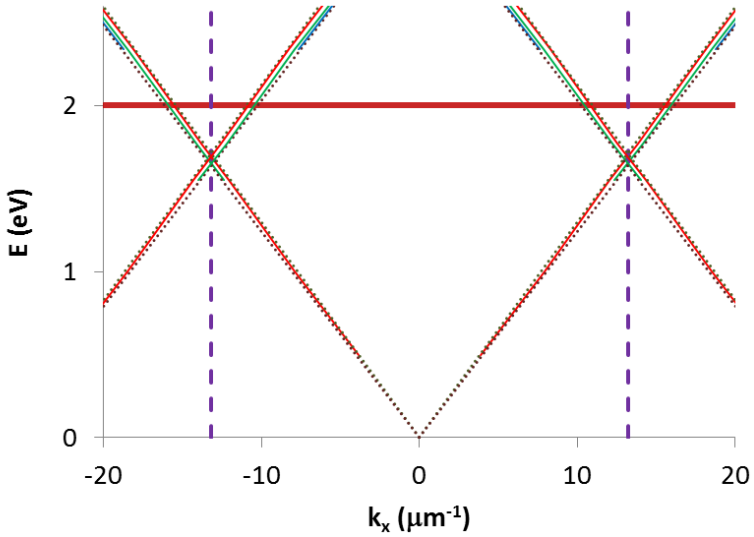

Fig. 3. Diagram of energy vs parallel wave vector showing the dispersion of Rayleigh anomalies and guided modes for a waveguide with refractive index n_2 = 1.59 coupled to a lattice with lattice constant Λ = 238 nm between media with n_1 = 1 and n_3 = 1.52. Dotted lines: Rayleigh anomalies for n = 1.52 and 1.59, thin solid lines: waveguide modes. Vertical purple lines: border of 1st Brillouin zone.The horizontal red line shows the emission energy of interest.

In Fig. 3, the intersections between the horizontal red line and the lines describing the resonances correspond to high emission intensity. From the parallel wave vector at these points, $k_x = 2\pi / \lambda n_3 \sin\theta$, the emission polar angle θ can be found in the medium of refractive index n_3 into which emission takes place.

If we aim at enhancing the emission at wavelength λ, the angle of highest emission intensity for a Rayleigh anomaly can be estimated from the condition

$$\lambda / \Lambda = | \pm n_3 \sin\theta \pm n_{2,3} | \qquad (1)$$

In this equation, Λ is the relevant lattice constant and $n_{2,3}$ is the refractive index of the medium supporting the Rayleigh anomaly. In the simple case of a periodic array on top of a substrate, it equals the index n_3 of the substrate. It is also possible to consider the thin layer of index n_2 deposited on top of the substrate and particles. If n_2 is higher than n_3, the thin layer

#251615 Received 9 Oct 2015; revised 22 Dec 2015; accepted 26 Dec 2015; published 7 Jan 2016

may support one or more waveguide modes. For a waveguide mode, diffraction is similarly possible under the constraints of parallel wave-vector conservation.

We are looking for the situation that the emitted radiation stays guided in the medium with index n_3, implying $\theta_c < \theta < 90^o$, where $\theta_c = \sin^{-1}(1/n_3)$ is the critical angle for total reflection (= 41° for n_3 = 1.52). Equation (1) can be used to estimate the optimum period. It yields that the lattice constant Λ should be either in the range $\lambda/(n_3 + n_{2,3}) < \Lambda < \lambda/(1 + n_{2,3})$ (as is the case in Fig. 3), or in the range $\lambda/(n_{2,3} - 1) < \Lambda < \lambda/(n_{2,3} - n_3)$. For a hexagonal lattice, the relevant (minimum and maximum) lattice constants are $\Lambda_1 = \frac{1}{2} p\sqrt{3}$ (along k_x) and $\Lambda_2 = \frac{3}{4} p$ (along k_y), where p is the lattice period. For a small lattice constant (Fig. 3), this would imply that the period p should be in the range $\frac{1}{3}\lambda/(n_3 + n_{2,3}) < p < 2/\sqrt{3}\,\lambda/(1 + n_{2,3})$.

In Section 2.2, we will consider the case with n_2 = 1.59 (polystyrene), n_3 = 1.52 (glass). Furthermore, we will take an emission wavelength λ = 620 nm. This is an interesting wavelength of red light in solid-state lighting since the eye sensitivity is appreciable at this wavelength and combining this red emission with blue and green leads to high-quality white light. This set of parameters implies that 266 < p < 276 nm for a hexagonal lattice.

2.2 Experiments

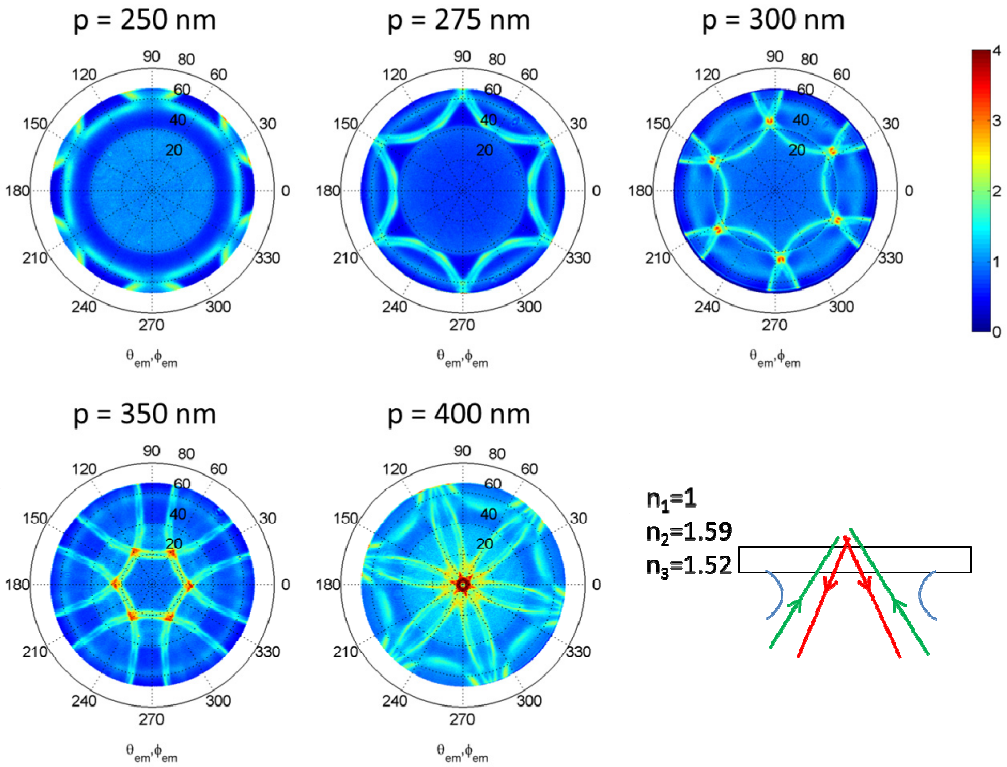

Fig. 4. Angular dependent (up to 80° azimuthal angle) photoluminescence enhancement at λ = 620 nm of a luminescent layer (thickness = 700 nm) on top of a hexagonal array of Al particles with various periods p. In the case of p = 400 nm, the maximum enhancement is 8, but for comparison the same scale is used in all panels. The inset shows the schematic experimental set-up in the Fourier microscope, with the incident light entering and the luminescent light exiting via an immersion-oil objective.

#251615 Received 9 Oct 2015; revised 22 Dec 2015; accepted 26 Dec 2015; published 7 Jan 2016

As an experimental assessment of the validity of our estimates, we have measured the angle-dependent emission into glass from luminescent layers on hexagonal arrays of nanoparticles. We did experiments for a series of 3 × 3 mm^2 hexagonal arrays of aluminium particles with various periods p on a glass substrate and on top of it, as emissive layer, a 700 nm thick layer of polystyrene (n = 1.59) containing 3 weight % of the organic luminescent dye F305 (BASF). This dye has a broad emission spectrum between wavelengths of ca. 550 and 700 nm. The aluminium particles have a truncated conical shape with a height of 150 nm, a width of 140 nm (bottom) and 80 nm (top). See reference [6] for details of manufacturing.

The angle-dependent emission into glass was measured with a Fourier microscope [15,16] using 532 nm epifluorescence illumination, a dichroic filter (Chroma, cut on 560 nm), a bandpass filter at 620 (± 10) nm (Thorlabs), and an immersion objective with NA = 1.4 (Nikon Plan Apo VC, 100X, immersion oil with refractive index 1.52), on a sensitive Hamamatsu Orca-Flash 4 CMOS camera. Fourier images at select pitches are displayed in Fig. 4, showing the photoluminescence enhancement, *i.e.*, the photoluminescence intensity with respect to that of a sample with the same polystyrene layer thickness and dye-doping, but without the presence of the metal nanoparticles. As can be seen, the angular range with enhanced emission is at larger polar angle for smaller periods and occurs in the form of sharply delineated, intersecting curves in a six-fold symmetry. As discussed above (Section 2.1), in a $k_{//}$ representation, the curves are strictly circles with radius $n_{\text{eff}}\, 2\pi/\lambda$ [Fig. 2(b)], with the effective waveguide mode index n_{eff} = 1.525. For a period around 400 nm, enhanced forward emission takes place, like in previous reports [12,13]. For a period p = 275 nm, enhanced emission is seen for $\theta > 41°$, which is the desired angular range for emission in glass with n = 1.52, in accordance with the above considerations.

3. Thickness optimization

We concentrate on the case with 275 nm period. Having fixed the period, we performed electromagnetic simulations using the finite-element method (FEM) [17] to find the optimal layer thickness, yielding maximal sideward emission at wavelength λ = 620 nm. The calculations were done for an incident beam with this wavelength and varying angle of incidence. According to the reciprocity theorem, the intensity calculated in this way at a certain position in the luminescent layer is equal to the intensity in the far field from an emitter at the same position in the layer. By integrating the intensity over all luminophore positions in a unit cell of the layer, the total (relative) luminescent intensity is obtained.

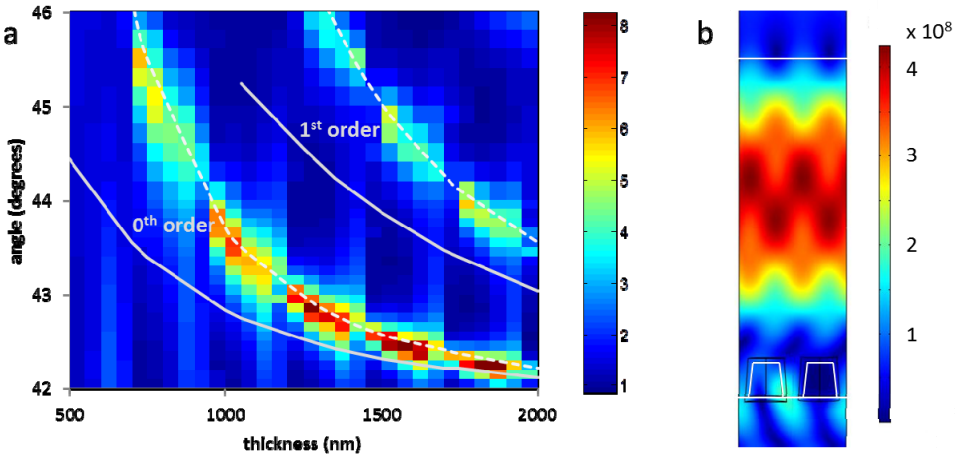

Fig. 5. (a) Photoluminescence enhancement for s-polarized light as a function of dye-layer thickness and polar angle for plasmonic structure (at φ = 0°). Indicated are the positions for the waveguide modes of order 0 and 1 (and diffraction order 1) calculated without (solid lines) and with a metal layer (dashed lines). (b) Cross section of two unit cells (thickness = 1500 nm) showing absolute value of electric field due to light at θ = 42.5°, φ = 0°.

#251615 Received 9 Oct 2015; revised 22 Dec 2015; accepted 26 Dec 2015; published 7 Jan 2016

In Fig. 5(a) the results are shown for the polar angle into glass $42° < \theta < 46°$ and azimuth angle $\varphi = 0°$ (i.e., along k_x). The various bands in this figure are due to diffraction into the waveguide modes in the luminescent layer with refractive index 1.59 between air at one side and glass with aluminium nanoparticles at the other side. To rationalize the dispersion of these modes, we have calculated the guided modes of a simplification of the full structure to just a three-layer stratified system [14]. In this approximation, two extremes are on one hand to ignore the metal particles, or on the other hand to take them as a fully reflective substrate. The positions of these modes are shown, calculated for the cases of air / luminescent layer / glass (solid lines) and air / luminescent layer / metal (dashed lines). In the latter case, the layer thickness is taken to be 150 nm less to correct for the metal particles, whereas the absorption of the metal is not taken into account. The angles are calculated from the parallel wave vector assuming 1st order diffraction. It can be seen that the fundamental (0th) waveguide order supports the strongest emission enhancement. A cross section of the structure for the case of 1500 nm thickness of the luminescent layer is shown in Fig. 5(b). Here the electric field amplitude is shown from an FEM calculation of an electromagnetic plane wave with $\lambda = 620$ nm incident at $\theta = 42.5°$, $\varphi = 0°$. According to the reciprocity theorem, the regions of highest intensity correspond to regions contributing most to the emission. For the parameter set used in this simulation, the main intensity due to the waveguide mode is concentrated in a region in the luminescent layer, away from the metallic particles.

The intensity behaviour of the 0th waveguide order in Fig. 5(a) shows, apart from weak oscillations due to thickness fringes, that the emission enhancement becomes stronger with increasing thickness and reaches a broad maximum between 1100 and 1800 nm. This increase of the emission enhancement is due to the well-known behaviour of the confinement factor, *i.e.*, the fraction of electromagnetic energy that resides in the central high-index dye-doped layer, which increases with thickness [14]. For very large thickness, the overlap between the waveguide mode and the metal particles is so small that there is hardly any coupling between them [10], which reduces the outcoupling of the emitted radiation.

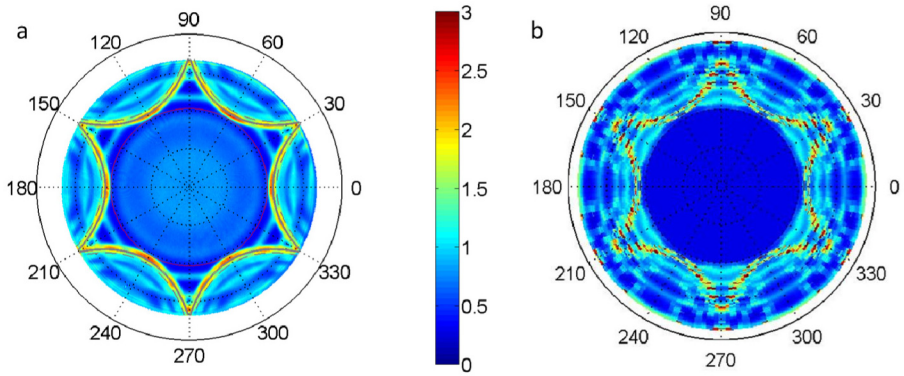

Fig. 6. Measured (a) and simulated (b) angular dependence of photoluminescence enhancement at $\lambda = 620$ nm for a luminescent layer (thickness = 1500 nm) on top of a hexagonal array of Al particles with period 275 nm.

To check the above explanation and to obtain more insight in the angular dependence of the emission, we have performed experiments and more detailed angle-dependent FEM simulations. We use a sample of a hexagonal array of aluminium nanoparticles as described above with pitch 275 nm, with on top of it a 3 weight % dye-doped polystyrene layer of 1500 nm thickness. Figure 6(a) shows the angle-dependent emission into glass, measured in the same way as in Fig. 4. Figure 6(b) shows the corresponding simulated results, calculated as indicated above using reciprocity. Figure 7 shows both measured and simulated data as a function of polar angle. Figures 7(a) and 7(b) correspond to the sample with the hexagonal array at azimuth angles 0° and 90°, respectively, while Fig. 7(c) shows the emission of the sample with the same polystyrene layer thickness and dye-doping but without the presence of

#251615 Received 9 Oct 2015; revised 22 Dec 2015; accepted 26 Dec 2015; published 7 Jan 2016

the metal nanoparticles. Note that the enhancement data of Fig. 6 are obtained by taking the ratio between the intensities of the nanostructured sample [Figs. 7(a) and 7(b)] and the unstructured sample [Fig. 7(c)] at the same angle. The intensity scale at the right vertical axis of Fig. 7 is relative to that of the unstructured sample at normal emission and the measured and simulated intensities are aligned at 0°.

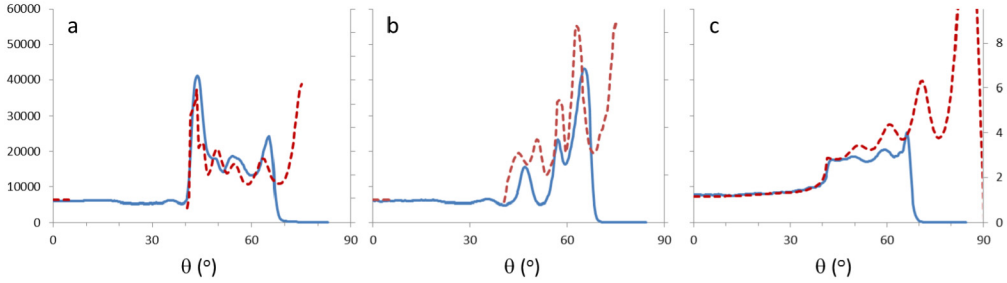

Fig. 7. Photoluminescence intensities as a function of polar angle for a 1500 nm thick luminescent layer on glass with a hexagonal array of Al particles with period 275 nm for φ = 0° (a) and φ = 90° (b) and for such a layer without nanostructure (c): measured (counts/s, blue solid line) and simulated (relative units, red dashed line). The vertical scales are the same for all panels.

Compared to the experiment for a thin polymer layer with the same lattice period (Fig. 4, p = 275 nm), the data in Fig. 6(a) show a similar six-fold structure, but with the higher photoluminescence enhancement aimed for at angles in the desired angular range of $\theta > 41°$. With regard to the calculations, it is computationally expensive to provide a denser sampling of angles, since each angle requires approximately 30 minutes of simulation time (the simulations were performed with COMSOL 4.4 [17] using its MPI-based parallel solvers on 35 HP server blades, type 'ProLiant BL460c Gen8', and using two cores per blade at 2.6 GHz each). The overall agreement between experiment and simulations is good, both in intensities and peak positions. In Fig. 7(c), the intensity for the reference sample increases by a factor of two for polar angles larger than 41°, the critical angle for escape in air. It shows thickness fringes, which are visible as well in the nanostructured sample. The latter [Figs. 7(a) and 7(b)] in addition shows peaks due to waveguide modes (cf. Figure 3), which are a factor two to three more intense than the intensity for the reference sample. Hence it is possible to emit an appreciable fraction of the luminescent light into the desired angular range; analysis of our results shows that this fraction is 75%.

4. Conclusions

By choosing a proper period of a plasmonic nanoparticle array it is possible to tune the emission angles from a thin luminescent layer in proximity with the array. We have shown that, for an emission wavelength of 620 nm and emission in glass at angles larger than 41°, the optimal period is around 275 nm. For the considered luminescent material (n = 1.59), the optimal thickness is around 1500 nm. The layer acts as a multimode waveguide from which light is preferentially emitted in the desired angular range.

Our experiments and simulations have been made for two-dimensional hexagonal arrays, in which case the emission pattern is highly symmetric. The results are equally valid for other symmetries. For instance, in case of a one-dimensional line grating with period 238 nm, the emission pattern of Fig. 7(a) will be obtained. The two-dimensional configuration is expected to find application in light tiles, whereas the one-dimensional configuration is potentially useful for high-brightness side-emitting light sources. Further possible applications are in luminescent solar concentrators, in which sunlight is converted to longer-wavelength light that is guided to small solar cells [18–21]. In that case, using directional emission, escape losses could be reduced.

#251615 Received 9 Oct 2015; revised 22 Dec 2015; accepted 26 Dec 2015; published 7 Jan 2016

Acknowledgements

This work is supported by: NanoNextNL, a micro and nanotechnology consortium of the Government of the Netherlands and 130 partners; the Dutch Technology Foundation STW, which is part of the Netherlands Organisation for Scientific Research (NWO), and which is partly funded by the Ministry of Economic Affairs; the Foundation for Fundamental Research on Matter (FOM), which is financially supported by the Netherlands Organization for Fundamental Research (NWO); the Industrial Partnership Program between Philips and FOM.

#251615 Received 9 Oct 2015; revised 22 Dec 2015; accepted 26 Dec 2015; published 7 Jan 2016